

advances.sciencemag.org/cgi/content/full/7/1/eabd6322/DC1

Supplementary Materials for

Cardiolipin content controls mitochondrial coupling and energetic efficiency in muscle

Alexandre Prola, Jordan Blondelle, Aymeline Vandestienne, Jérôme Piquereau, Raphaël G. P. Denis, Stéphane Guyot, Hadrien Chauvin, Arnaud Mourier, Marie Maurer, Céline Henry, Nahed Khadhraoui, Cindy Gallerne, Thibaut Molinié, Guillaume Courtin, Laurent Guillaud, Mélanie Gressette, Audrey Solgadi, Florent Dumont, Julien Castel, Julien Ternacle, Jean Demarquoy, Alexandra Malgoyre, Nathalie Koulmann, Geneviève Derumeaux, Marie-France Giraud, Frédéric Joubert, Vladimir Veksler, Serge Luquet, Frédéric Relaix*, Laurent Tiret*, Fanny Pilot-Storck*

*Corresponding author. Email: fanny.storck@vet-alfort.fr (F.P.-S.); laurent.tiret@vet-alfort.fr (L.T.); frederic.relaix@inserm.fr (F.R.)

Published 1 January 2021, *Sci. Adv.* 7, eabd6322 (2021)
DOI: 10.1126/sciadv.abd6322

The PDF file includes:

Tables S1 to S7
Supplementary Listing S1
Figs. S1 to S6

Other Supplementary Material for this manuscript includes the following:

(available at advances.sciencemag.org/cgi/content/full/7/1/eabd6322/DC1)

Table S3

Table S1: Anatomical parameters of WT and *Hacd1*-KO mice after normal or high fat diet.
Related to Figures 1 and S1.

	WT ND	<i>Hacd1</i> -KO ND	WT HFD	<i>Hacd1</i> -KO HFD
Eviscerated BW (g)	29.9 ± 1.4	26.3 ± 1.5	33.1 ± 2.1	25.8 ± 1.3 *
Initial BW (g)	29.3 ± 0.9	26.3 ± 0.5 **	29.6 ± 0.6	25.4 ± 0.7 ***
Final BW (g)	32.4 ± 1.2	28.8 ± 0.4 **	44.2 ± 1.3 \$\$\$	31.4 ± 1.4 ***
BW gain (g)	3.1 ± 0.6	2.5 ± 0.3	14.6 ± 1.0 \$\$\$	6.3 ± 1.0 ***\$
BW gain (%)	10.4 ± 1.8	9.7 ± 1.1	49.5 ± 3.2 \$\$\$	25.3 ± 3.9 ***\$\$
Tibial length (cm)	1.78 ± 0.03	1.80 ± 0.04	1.74 ± 0.02	1.74 ± 0.02
Heart weight (mg)	130.3 ± 4.9	120.1 ± 3.6	153.7 ± 7.6 \$	130.7 ± 13.5 **
Lung weight (mg)	185.8 ± 16.4	164.9 ± 11.6	273.3 ± 27.9	221.2 ± 9.9
Liver weight (mg)	1633.7 ± 85.1	1309.6 ± 39.0	1698.5 ± 118.2	1132.7 ± 103.1 \$
Kidney weight (mg)	214.9 ± 11.2	185.9 ± 7.2	203.8 ± 5.8	205.2 ± 3.9
Tibial anterior (mg)	46.1 ± 1.3	37.5 ± 0.9 **	47.9 ± 1.8	40.8 ± 1.3 ***
Gonadal fat pad (mg)	416 ± 82	279 ± 90	2182 ± 244 \$\$\$	1079 ± 244 **\$
Retroperitoneal fat pad (mg)	157.2 ± 47.3	94.3 ± 16.5	927.8 ± 83.0 \$\$\$	353.3 ± 91.2 ***
Mesenteric fat pad (mg)	567.2 ± 27.5	504.0 ± 42.9	942.7 ± 121.2 \$\$	452.0 ± 102.7 **
BAT weight (mg)	133.9 ± 16.9	79.3 ± 5.8 **	283.2 ± 26.2 \$\$\$	174.1 ± 26.9 \$\$\$**
HW/BW	4.21 ± 0.11	4.83 ± 0.14 *	3.52 ± 0.15 \$	3.96 ± 0.22 \$\$
Lung /BW	5.98 ± 0.44	6.61 ± 0.43	6.24 ± 0.49	6.66 ± 0.27
Liver/BW	52.63 ± 1.39	52.53 ± 0.82	38.57 ± 2.06 \$	33.45 ± 1.76 \$
Kidney/BW	6.92 ± 0.13	7.46 ± 0.26	4.70 ± 0.21 \$	6.24 ± 0.33
TA/BW	1.75 ± 0.03	1.52 ± 0.04 **	1.11 ± 0.02 \$\$\$	1.23 ± 0.00 \$\$\$
Gonadal fat pad/BW	11.85 ± 2.03	9.13 ± 0.72	53.31 ± 5.04 \$\$\$	34.26 ± 5.87 *\$
Retroperitoneal fat pad/BW	4.44 ± 1.23	3.01 ± 0.37	22.81 ± 1.34 \$\$\$	11.13 ± 2.31 ***\$\$\$
Mesenteric fat pad/BW	16.37 ± 0.59	16.27 ± 0.37	23.13 ± 1.94 \$	14.31 ± 2.35 *
BAT/BW	4.25 ± 0.40	3.18 ± 0.21 *	6.43 ± 0.50 \$\$	5.05 ± 0.57 \$\$*

Table S2: Echocardiographic parameters of WT and *Hacd1*-KO mice.
Related to Figures 2 and S2.

	WT	<i>Hacd1</i> -KO
EF(%)	81.2 ± 2.3	83 ± 2.2
FS (%)	44.8 ± 2.5	46.7 ± 2.7
HR (bpm)	631 ± 9	624 ± 17
LVd (mm)	2.73 ± 0.11	2.88 ± 0.05
LVs (mm)	1.51 ± 0.10	1.54 ± 0.10
IVSd (mm)	0.83 ± 0.04	0.78 ± 0.03
IVSs (mm)	1.43 ± 0.05	1.44 ± 0.05
PWd (mm)	0.82 ± 0.03	0.80 ± 0.04
PWs (mm)	1.36 ± 0.07	1.48 ± 0.05
Strain rate ant (unit/s)	25.64 ± 1.40	23.25 ± 1.33
Strain rate post (unit/s)	25.91 ± 1.60	23.75 ± 1.08

Table S3: Proteomic dataset and Panther analysis.
Related to Figure S2.

See Table S3 Excel File .

Table S4: Mitochondrial respiration rates.

Related to Figures 3 and S3.

Mitochondrial respiration rates for different complexes in WT or *Hacd1*-KO mice superficial *gastrocnemius* and *soleus* permeabilized muscle fibers.

	WT Gast. (6)	<i>Hacd1</i>-KO Gast. (6)	P
Vo	2.16 ± 0.29	4.10 ± 0.45	0.003
Complex I	11.06 ± 0.89	9.37 ± 1.03	0.235
Complex I+II	16.11 ± 1.56	12.26 ± 1.42	0.089
Complex II	5.71 ± 0.54	3.45 ± 0.44	0.006
Ratio CxII/CxI	0.52 ± 0.04	0.37 ± 0.05	0.020
ACR (Complex I/Vo)	5.73 ± 0.94	2.71 ± 0.68	0.007
	WT Soleus (6)	<i>Hacd1</i>-KO Soleus (6)	P
Vo	4.21 ± 0.49	7.92 ± 0.55	<0.001
Complex I	19.72 ± 2.31	16.05 ± 1.39	0.263
Complex I+II	25.07 ± 2.78	23.46 ± 2.28	0.652
Complex II	13.78 ± 2.93	15.37 ± 1.62	0.534
Ratio CxII/CxI	0.68 ± 0.03	0.67 ± 0.05	0.878
ACR (Complex I/Vo)	4.83 ± 0.35	3.05 ± 0.28	<0.001
	WT Heart (4)	<i>Hacd1</i>-KO Heart (4)	P
Vo	5.40 ± 0.30	5.62 ± 0.32	0.611
Complex I	27.25 ± 1.28	29.67 ± 1.83	0.299
Complex I+II	37.34 ± 2.76	44.59 ± 3.80	0.207
ACR (Complex I/Vo)	5.22 ± 0.42	5.39 ± 0.38	0.782

Mitochondrial substrate utilization in WT or *Hacd1*-KO mice superficial *gastrocnemius* and *soleus* permeabilized muscle fibers.

	WT Gast. (6)	<i>Hacd1</i>-KO Gast. (6)	P
Vo	0.97 ± 0.16	2.07 ± 0.14	<0.001
Palmitoyl-CoA	2.27 ± 0.30	3.06 ± 0.35	0.043
+ octanoate	2.29 ± 0.36	3.10 ± 0.30	0.026
+ pyruvate	7.37 ± 0.52	7.49 ± 0.36	0.851
+ Glutamate/Succinate	10.27 ± 0.98	11.18 ± 0.62	0.425
ACR (PCoA/Vo)	3.07 ± 0.61	1.52 ± 0.16	0.003
% fatty acids	27.33 ± 4.81	28.33 ± 2.47	0.845
% pyruvate	59.03 ± 5.06	67.90 ± 2.67	0.112
% PCoA/Octanoate	97.52 ± 6.21	97.71 ± 1.76	0.975
	WT Soleus (6)	<i>Hacd1</i>-KO Soleus (6)	P
Vo	3.32 ± 0.81	6.04 ± 0.50	<0.001
Palmitoyl-CoA	12.83 ± 1.13	15.79 ± 1.03	0.049
+ octanoate	14.65 ± 0.75	17.89 ± 0.89	0.011
+ pyruvate	18.88 ± 1.17	20.44 ± 1.82	0.583
+ Glutamate/Succinate	24.14 ± 1.54	25.14 ± 1.90	0.931
ACR (PCoA/Vo)	3.85 ± 0.22	2.77 ± 0.26	0.004
% fatty acids	61.96 ± 3.50	72.69 ± 2.76	0.025
% pyruvate	78.48 ± 2.14	81.01 ± 2.12	0.583
% PCoA/Octanoate	86.03 ± 4.72	89.22 ± 5.93	0.678

Mitochondrial respiration rates in isolated mitochondria from WT or *Hacd1*-KO mice TA.

	WT (4)	<i>Hacd1</i>-KO (4)	P
Phosphorylating (State 3)	101.55 ± 19.72	48.03 ± 7.20	0.044
State 4	10.90 ± 0.87	12.75 ± 2.01	0.432
RCR	9.14 ± 1.24	3.12 ± 0.48	0.004
Non-phosphorylating	14.34 ± 1.70	11.25 ± 1.04	0.172
Uncoupled	189.42 ± 16.95	160.78 ± 16.48	0.153
Cyt-C stimulation (%)	7.80 ± 3.80	8.57 ± 3.98	0.667
VO₂ (for ATP/O determination)	129.87 ± 6.80	96.62 ± 10.57	0.038
ATP production (for ATP/O determination)	2.02 ± 0.24	0.89 ± 0.22	0.011

Table S5: Non-linear mixed-effects models of the fluorescence decay of TMA-DPH.
Related to Figure S6.

Non-linear mixed-effects models of the fluorescence decay from the analyses of mtIM.

	Dependent variable: Experimental response (event count/ns)			
	A	B1	B2	C
θ_1	0.455*** (0.153)	0.505*** (0.153)		
B_1	0.025*** (0.001)		0.025*** (0.001)	
θ_2	-2.852*** (0.242)	-2.631*** (0.257)		
B_2	0.0002* (0.0001)		0.0001* (0.0001)	
θ_3	-0.697*** (0.087)	-0.667*** (0.094)		
B_3	0.016*** (0.001)		0.016*** (0.001)	
B_1 (inter.)		0.029*** (0.002)		0.029*** (0.002)
B_1 (WT)		-0.007*** (0.002)		-0.007*** (0.002)
B_2 (inter.)		0.001*** (0.0002)		0.0005*** (0.0002)
B_2 (WT)		-0.0004 (0.0003)		-0.0004 (0.0003)
B_3 (inter.)		0.018*** (0.001)		0.018*** (0.001)
B_3 (WT)		-0.002 (0.002)		-0.002 (0.002)
θ_1 (inter.)			0.752*** (0.160)	0.846*** (0.172)
θ_1 (WT)			-0.647*** (0.226)	-0.708*** (0.243)
θ_2 (inter.)			-2.629*** (0.316)	-2.432*** (0.336)
θ_2 (WT)			-0.509 (0.448)	-0.549 (0.476)
θ_3 (inter.)			-0.727*** (0.121)	-0.692*** (0.126)
θ_3 (WT)			0.040 (0.171)	0.028 (0.178)
Obs.	57,344	57,344	57,344	57,344
Log Likelihood	-136,223.600	-136,134.000	-136,268.900	-136,157.800
Akaike Inf. Crit.	272,475.300	272,301.900	272,571.900	272,355.600
Bayesian Inf. Crit.	272,600.700	272,454.200	272,724.100	272,534.800

Table S6: Sequence of qPCR primers used in this study.

Related to Materials and methods.

Gene	Forward primer	Reverse primer
<i>Acadm</i>	CCGTTCCCTCTCATCAAAAG	ACACCCATACGCCAACTCTT
<i>Acadvl</i>	TGGGCCTCTCTAATACCCAGT	TCCCAGGGTAACGCTAACAC
<i>Cd36</i>	CCACTGTGTACAGACAGTTTG	GCTCAAAGATGGCTCCATTG
<i>Catalase</i>	CCTCGTTCAGGATGTGGTT	TCTGGTGATATCGTGGGTGA
<i>Coxl</i>	CACTAATAATCGGAGCCCCA	TTCATCCTGTTCTGCTCCT
<i>Cpt1</i>	TCACCTGGGCTACACGGAGA	TCGGGGCTGGCCTACACTT
<i>Cpt2</i>	ACCTGCTCGCTCAGGATAAA	AAACGACAGAGTCTCGAGCAG
<i>Fas</i>	GCAAGTGCAGCCTGAGGGAC	ACAGCCTGGGTCATCTTGC
<i>Gpx1</i>	GTTTCCCGTGCAATCAGTTC	TCACTTCGCACCTCTCAAACA
<i>Hadha</i>	GCTTGGGAGGGAGGACTTGA	AGCAACACTTCAGGGACACC
<i>Nrf1</i>	TTACTCTGCTGTGGCTGATGG	CCTCTGATGCTTGCCTCGTCT
<i>Pex11a</i>	TCAAGAGGCTGGAGACCAGT	CGGTTGAGGTTGGCTAATGT
<i>Pex19</i>	TGTACCCATCCCTGAAGGAG	TGTGCTGCTGCTGGTACTTC
<i>Polr2a</i>	CAACATGCTGACAGATATGACC	TGATGATCTTCTTCTTGTCTG
<i>Ppara</i>	AAGTGCCTGTCTGTCGGAT	GCTTCGTGGATTCTCTTGCC
<i>Ppard</i>	GGGGACCAGAACACACGCTT	CCGCACACCCGACATTCCAT
<i>Ppargc1a</i>	CACCAAACCCACAGAGAACAG	GCAGTTCCAGAGAGTTCCACA
<i>Ppargc1b</i>	TGGAAAGCCCTGTGAGAGT	TTGTATGGAGGTGTGGTGGG
<i>Rpl32</i>	GCTGCTGATGTGCAACAAA	GGGATTGGTGAECTCTGATGG
<i>Rplpo</i>	GCGACCTGGAAGTCCAACTA	TTGTCTGCTCCCACAATGAA
<i>Sod2</i>	AGGAGCAAGGTGCGTTACAG	GTAGTAAGCGTGCTCCCACA
<i>Scd1</i>	CTACATGACCAGCGCTCTG	CGTACACGTCATTCTGGAACG
<i>Scd2</i>	GTAATCAGCGCCCTGGGCAT	CATACACGTCATTCTGGAACGC
<i>Srebp-1c</i>	CTGGAGACATCGCAAACAAGCTG	TGAGGTTCAAAGCAGACTGCAG
<i>Tfam</i>	GCTGATGGGTATGGAGAAG	GAGCCGAATCATCCTTGC
<i>Ucp1</i>	AGGGAGAGAAACACCTGCC	GCATTCTGACCTTCACGACC
<i>Ucp2</i>	CAGATGTGGTAAAGGTCCGC	CAGAAGTGAAGTGGCAAGGG
<i>Ucp3</i>	ATGGTTGGACTTCAGCCCTC	TGGGGTGTAGAACTGCTTG

Table S7: Key resources table.
Related to Materials and methods.

REAGENT or RESOURCE	SOURCE	IDENTIFIER
Antibodies		
Rabbit anti-AMPK	Cell signaling	2532
Rabbit anti-phospho-AMPK	Cell signaling	2535
Rabbit anti-Citrate Synthase	Cell signaling	14309
Rabbit anti-UCP3	Abcam	ab10985
Mouse anti-ATP5A	Abcam	ab110413
Rabbit anti-VDAC	Custom	N/A
Mouse anti-β-actin	Santa Cruz	47778
Chemicals, Peptides, and Recombinant Proteins		
Sodium pyruvate	Sigma	P2256
Palmitoyl coenzyme A lithium salt	Sigma	P9716
L-Carnitine inner salt	Sigma	C0158
L-Glutamic acid potassium salt monohydrate	Sigma	G1501
L-(–)-Malic acid	Sigma	M6413
Sodium succinate dibasic	Sigma	14160
Adenosine 5'-diphosphate monopotassium salt dihydrate	Sigma	A5285
Adenosine 5'-triphosphate disodium salt hydrate	Sigma	A3377
β-Nicotinamide adenine dinucleotide, reduced disodium salt hydrate	Sigma	N8129
Carbonyl cyanide 4-(trifluoromethoxy)phenylhydrazone (FCCP)	Sigma	C2910
N,N,N',N'-Tetramethyl-p-phenylenediamine dihydrochloride	Sigma	T3134
(+)-Sodium L-ascorbate	Sigma	A7631
Magnesium chloride solution	Sigma	63069
Sodium azide	Sigma	S2002
Cytochrome c from equine heart	Sigma	C2506
Oligomycin from Streptomyces diastatochromogenes	Sigma	O4876
Digitonin	Sigma	D141
Saponin	Sigma	84510
Acetyl coenzyme A lithium salt	Sigma	A2181
Oxaloacetic acid	Sigma	O4126
5,5'-Dithiobis(2-nitrobenzoic acid)	Sigma	D8130
Trizma® base	Sigma	T1503
Potassium hexacyanoferrate(III)	Sigma	P3667
Bovine Serum Albumin	Sigma	A7030
D-(+)-Glucose	Sigma	G7021
Sodium dithionite	Sigma	1.06507
Dibasic potassium phosphate	Sigma	1551128
Potassium phosphate monobasic	Sigma	P5655
Sodium bicarbonate	Sigma	S5761
TRI Reagent®	Sigma	T9424
Nitrotetrazolium Blue chloride	Sigma	N6876
Menadione	Sigma	M5625
rac-Glycerol 1-phosphate disodium salt hydrate	Sigma	G2138
Glycerol	Sigma	G7757
Calcium chloride dihydrate	Sigma	C3881
Hepes sodium salt	Sigma	H7006
MOPS	Sigma	M1254
Ethylene glycol-bis(2-aminoethyl ether)-N,N,N',N'-tetraacetic acid	Sigma	03777
Hematoxylin Solution, Mayer's	Millipore	109249
Oil Red O	Sigma	O0625
Bolt™ 4-12% Bis-Tris Plus Gels, 17-well	Thermo Fisher Scientific	NW04127BOX
TMA-DPH (N,N,N-Trimethyl-4-(6-phenyl-1,3,5-hexatrien-1-yl)phenylammonium p-toluenesulfonate)	Sigma	T0775
cis-Aconitic acid	Sigma	A3412
Triton™ X-100	Sigma	T9284
Sodium pyrophosphate dibasic	Sigma	P8135
Acetoacetyl coenzyme A sodium salt hydrate	Sigma	A1625
Fluorescent mounting medium containing chromatin stain DAPI	Vectashield®	H-1200
Sodium cyanide	Sigma	431591
Rhodamine 123	Sigma	R8004

Perchloric acid	Sigma	311421
Cardiolipin from bovine heart	Sigma	C0563
TopFluor® Cardiolipin	Sigma	810286C
Egg PC	Sigma	131601C
Texas Red™ DHPE	Thermofischer	T1395MP
HEPES	Sigma-Aldrich	H3375-100G
Potassium Acetate	Sigma-Aldrich	P1190-500G
6-Aminocaproic acid	Sigma-Aldrich	A7824-25G
EDTA disodic	euromedex	EU0007-B
Glycerol	VWR	24388.295
Invitrogen™ Novex™ NativePAGE™ 3-12% Bis-Tris Protein Gels, 1.0mm, 10 well	Fisher Scientific	10064012
Digitonin	Merck	300410-5GM
D-(+)-Sucrose, ultrapure DNase RNase free	VWR	0335-500g
Tris-Base	Euromedex	200923-A
EGTA	Sigma-Aldrich	E3889-100G
Potassium chloride	Alfa Aesar	11595-A1
Magnesium Chloride, HexaHydrate	Euromedex	2189-B
KH2PO4 Potassium phosphate, monobasic, anhydrous	Euromedex	2018-A
Iodonitrotetrazolium	Sigma-Aldrich	I8377-1G
Diaminobenzidine	Sigma-Aldrich	32750-5G-F
Cytochrome c from bovine heart	Sigma-Aldrich	C2037-500MG
Critical Commercial Assays		
ATP Bioluminescence Assay Kit CLS II	Roche	11699695001
Pierce BCA	Thermo Fisher Scientific	23225
SuperSignal™ West Femto Maximum Sensitivity Substrate	Thermo Fisher Scientific	34095
Maxima First Strand cDNA Synthesis Kit for RT-qPCR	Thermo Fisher Scientific	K1641
Maxima SYBR Green qPCR Master Mix (2X), with separate ROX vial	Thermo Fisher Scientific	K0252
Rat/Mouse Insulin ELISA	Millipore	EZRMI-13K
Deposited Data		
Raw and analyzed data	This paper	github.com/hchauvin/prola2019
Uniprot Mus Musculus database	Uniprot	uniprot.org
GenBank sequence database	NIH	ncbi.nlm.nih.gov/genbank/
Experimental Models: Organisms/Strains		
Mouse: <i>Hacd1</i> -KO mice in the C57BL/6N genetic background	Home-made	ncbi.nlm.nih.gov/pubmed/26160855
Oligonucleotides		
Primers, see Table S6	This paper	N/A
Software and Algorithms		
ImageJ	NIH	fiji.sc
SigmaStat 3.0	Systat Software	systatsoftware.com
GraphPad	GraphPad Software	graphpad.com/company/
Algorithms for TMA-DPH decay analysis	This paper	github.com/ProlaLab/Prola2020.Sci.Adv
PANTHER Classification system	GENEONTOLOGY	http://pantherdb.org/
XTandem Pipeline	The Global Proteome Machine Organization	http://pappso.inra.fr/bioinfo/xtandempipeline

Supplemental Listing S1 | Final non-linear mixed effects models of the fluorescence decay of TMA-DPH on mitoplasts and whole mitochondria.
Related to Figure S6. (*in the R statistical language*).

```
1 library(nlme)
2
3 # Shared coefficients between Hacd1-KO and WT
4 model_A <- nlme(
5   Decay ~ ...,
6   fixed = theta1 + B1 + theta2 + B2 + theta3 + B3 ~ 1,
7   random = list(
8     File = pdDiag(B1 + B2 + B3 + theta1 + theta2 + theta3 ~ 1)
9   ),
10  weights = varConstPower(fixed = c(power = 0.5), const = 1, form = ~ fitted(.))
11 )
12
13 # Only Bs (resolving to mixing proportions) allowed to be different
14 # in Hacd1-KO and WT populations
15 model_B1 <- update(
16   model_A,
17   fixed = list(
18     theta1 + theta2 + theta3 ~ 1,
19     B1 + B2 + B3 ~ Population
20   )
21 )
22
23 # Only thetas (resolving to characteristic times) allowed to be different
24 model_B2 <- update(
25   model_A,
26   fixed = list(
27     theta1 + theta2 + theta3 ~ Population,
28     B1 + B2 + B3 ~ 1
29   )
30 )
31
32 # All coefficients allowed to be different
33 model_C <- update(
34   model_A,
35   fixed = theta1 + B1 + theta2 + B2 + theta3 + B3 ~ Population
36 )
```

Supplemental Table S1 | Anatomical parameters of WT and *Hacd1*-KO mice after normal or high-fat diet. Related to Figures 1 and S1.

Anatomical parameters measured after 9 wk of normal (ND) or high-fat diet (HFD). BW: body weight; initial and final: before and after the 9-wk period of ND or HFD, respectively; BW gain: difference between final and initial body weight; HW: heart weight; TA: *tibialis anterior* mass; GWAT, RWAT and MWAT: gonadal, retroperitoneal and mesenteric white adipose tissue weight, respectively; BAT: brown adipose tissue weight. Results are represented as mean \pm s.e.m.. $n = 9$. * $P < 0.05$; ** $P < 0.01$; *** $P < 0.001$ versus respective WT values. \$ $P < 0.05$; \$\$ $P < 0.01$; \$\$\$ $P < 0.001$ versus respective ND values.

Supplemental Table S2 | Echocardiographic parameters of WT and *Hacd1*-KO mice. Related to Figures 2 and S2.

Cardiac function of mice fed with normal diet was analyzed by echocardiography. EF: Ejection Fraction; FS: Fractional shortening; HR: Heart rate; LVd, LVs: Left Ventricle diameter in diastole and systole, respectively; IVSd, IVSs: interventricular septum thickness in diastole and systole, respectively; PWd, PWs: posterior wall thickness in diastole and systole, respectively. Strain rate was measured in unit/s (ant.) and (post.). Results are represented as mean \pm s.e.m.. $n = 8$ per group.

Supplemental Table S3 | Proteomic dataset and Panther analysis. Related to Figure S2.

Supplemental Table S4 | Mitochondrial respiration rates. Related to Figures 3 and S3.

Complex activity and substrate utilization unit is $\mu\text{molO}_2/\text{min/g}$ of dry mass of fibers or per g of protein for isolated mitochondria. Respiration rates in the presence of saturating pyruvate and ADP (Phosphorylating, State 3) and after complete ADP consumption (State 4). RCR: Respiratory Control Ratio. Respiration rates in the presence of oligomycin (Non-phosphorylating) and FCCP (Uncoupled). At the end of the experiment, cytochrome c was added to the medium (Cyt-C stimulation) to check that the stimulation of respiration did not exceed 10%, confirming the integrity of the outer mitochondrial membrane. Simultaneous measurement of respiration rates and ATP production in the presence of saturating pyruvate and ADP (State 3) for ATP/O determination. Values are given as mean \pm s.e.m.. Number in parentheses is the number of analyzed animals. Value for each animal was the mean of 1-3 independent analyses. For statistical analysis, unpaired t-test was used. ACR: Acceptor Control Ratio.

Supplemental Table S5 | Non-linear mixed-effects models of the fluorescence decay of TMA-DPH. Related to Figure S6.

Values are given as fixed effects \pm s.e for the variables defined in models A, B1, B2 and C (see *Materials and Methods*). More specifically, B_1 , B_2 and B_3 are scale coefficients for the three exponentials and θ_1 , θ_1 and θ_1 are monotonous parametrizations of characteristic times. For models B1, B2 and C, the variables are

regressed against the mice phenotype (WT or *Hacd1*-KO). The contrast matrix for this regression is given in the *Materials and Methods*. $P < 0.1$; $*P < 0.05$; $**P < 0.01$; $***P < 0.001$.

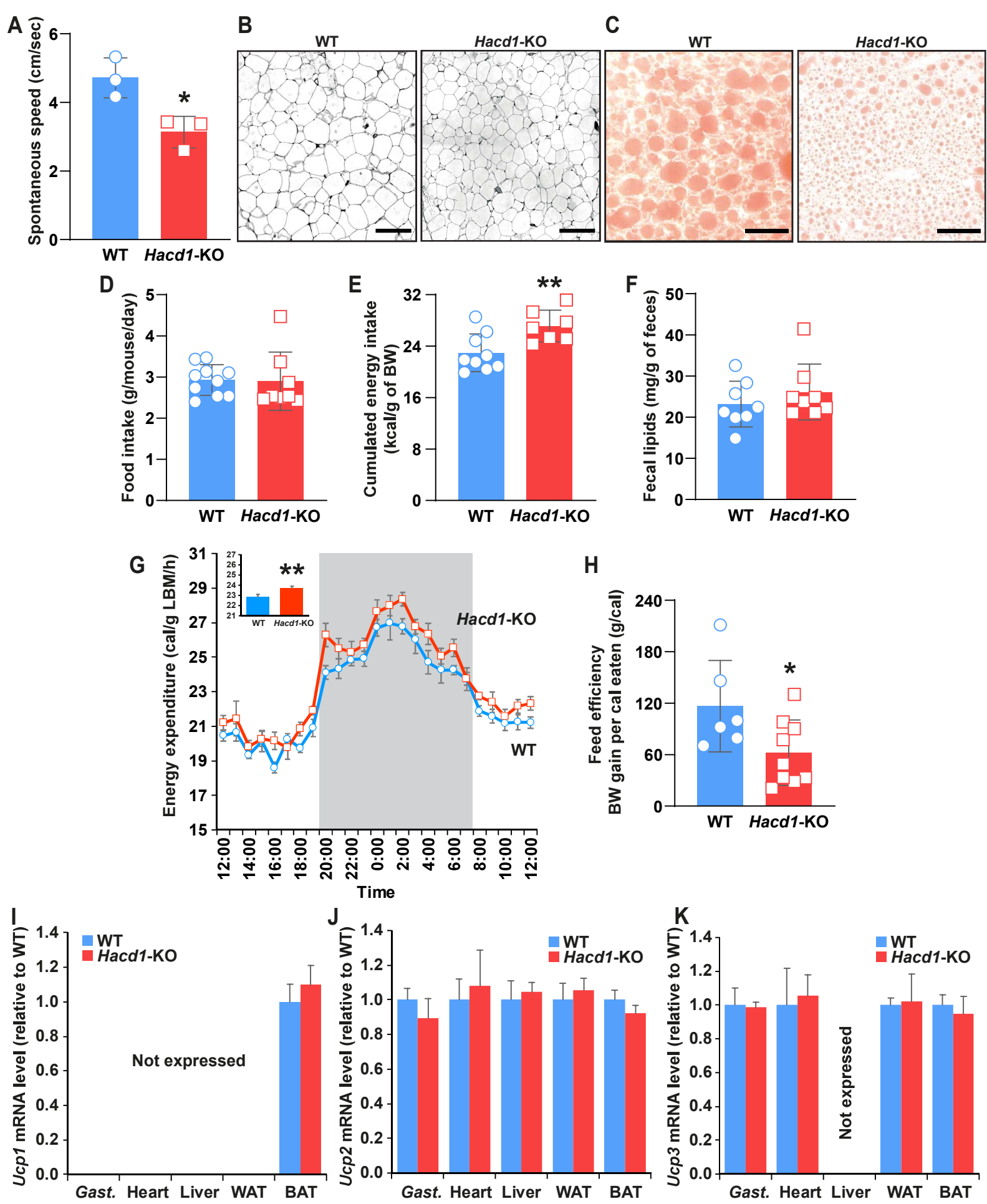
Supplemental Table S6 | Sequence of qPCR primers used in this study. Related to Materials and methods.

Supplemental Table S7 | Key resources table. Related to Materials and methods.

Supplemental Listing S1 | Final non-linear mixed effects models of the fluorescence decay of TMA-DPH on mitoplasts and whole mitochondria. Related to Figure S6.

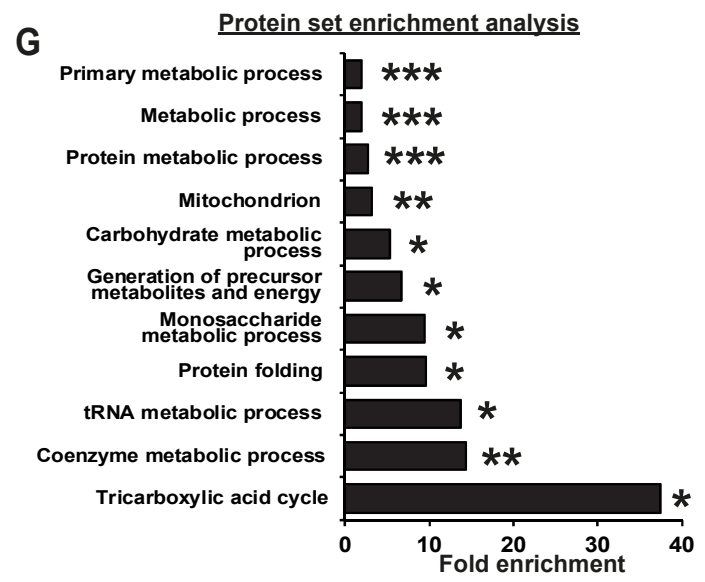
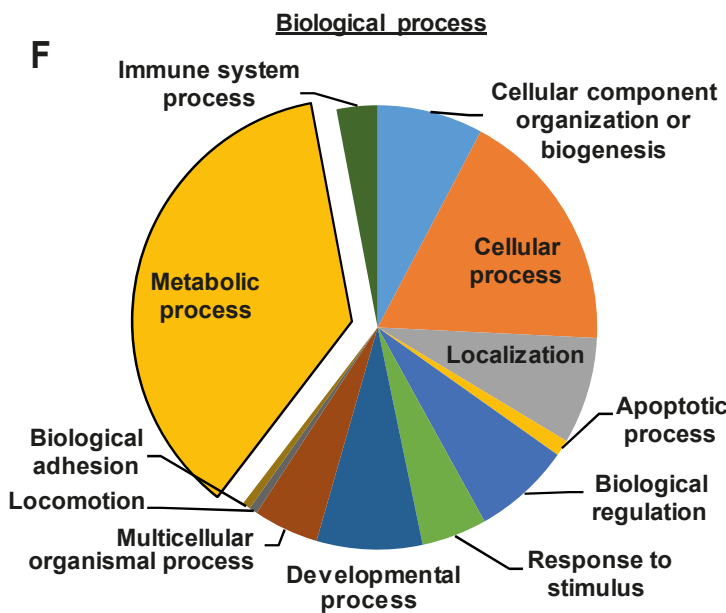
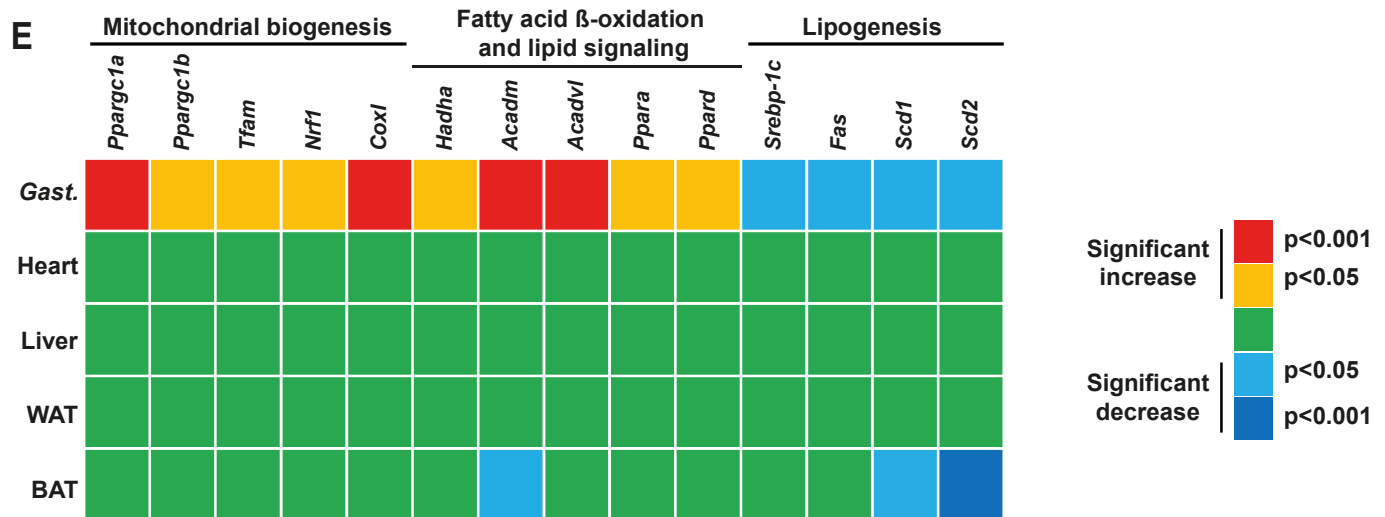
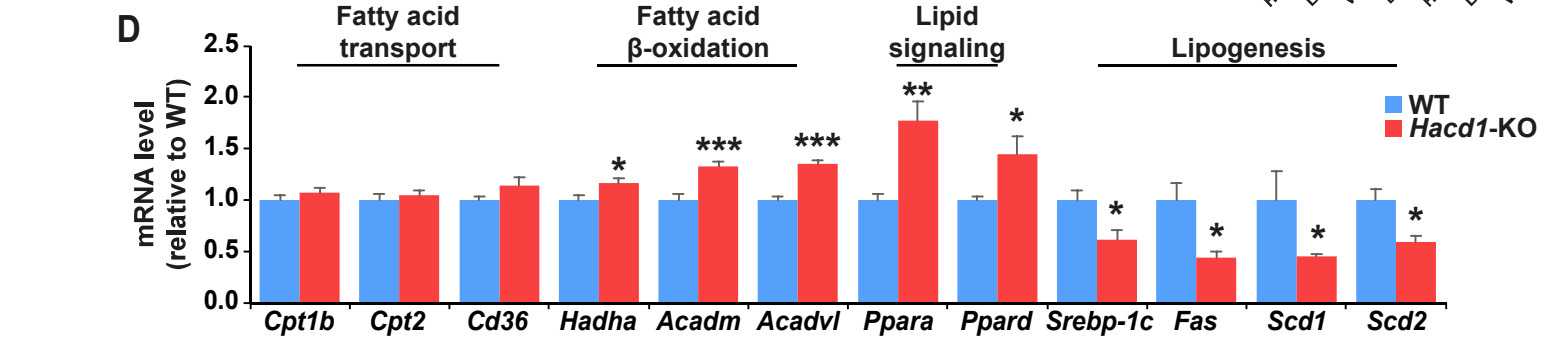
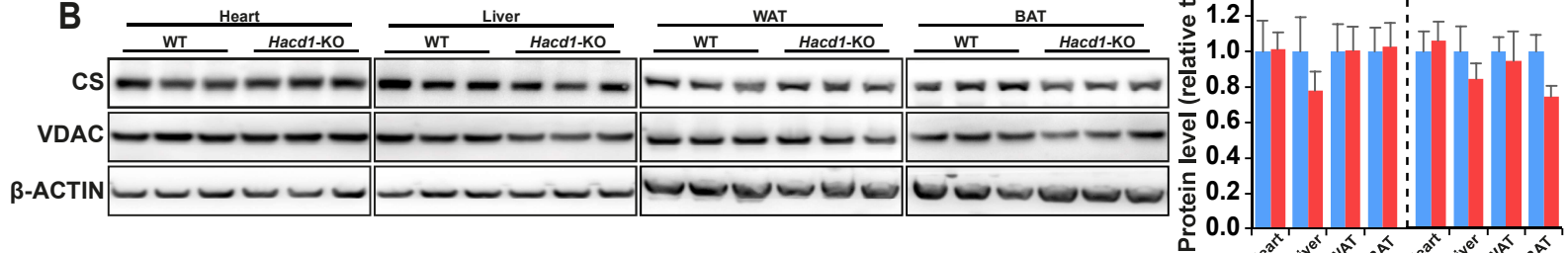
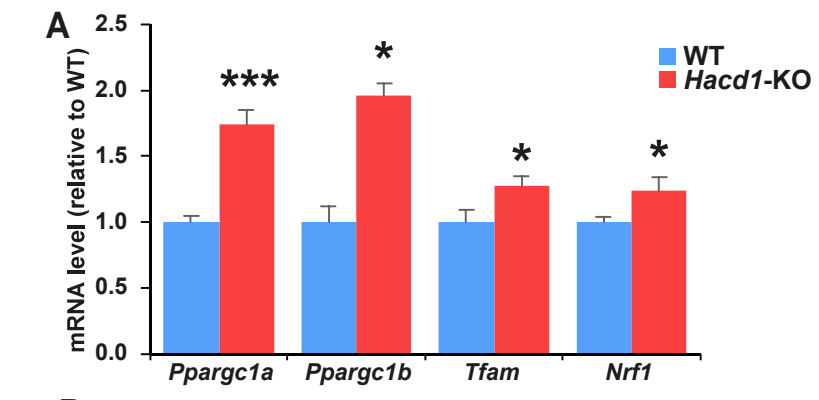
Specifics, given in the *R statistical language* for the **nlme** library, of the non-linear mixed effects models A, B1, B2 and C.

All the code is made available at github.com/ProlaLab/Prola2020.Sci.Adv with the appropriate tests and reproducible workflow (in addition, the releases are archived at DOI 10.5281/zenodo.1228112). The raw data is available upon request at DOI 10.5281/zenodo.4046133.



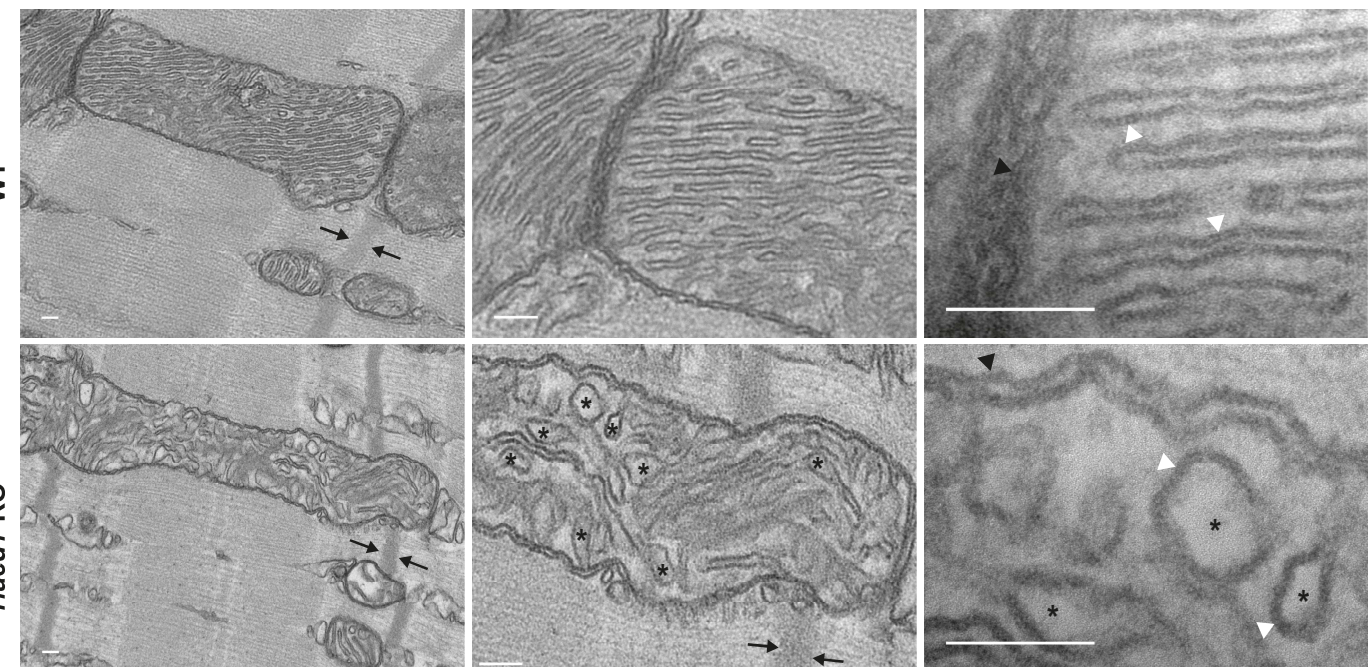
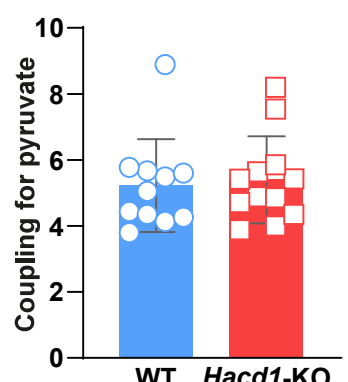
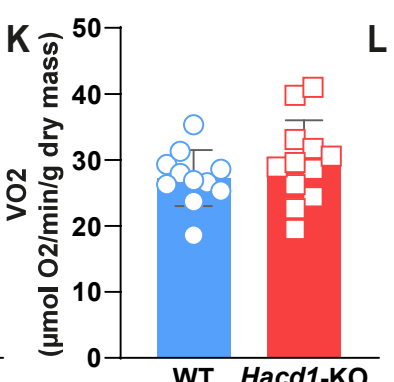
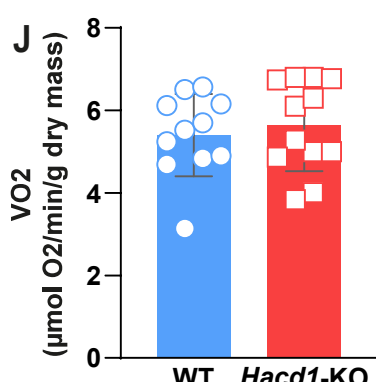
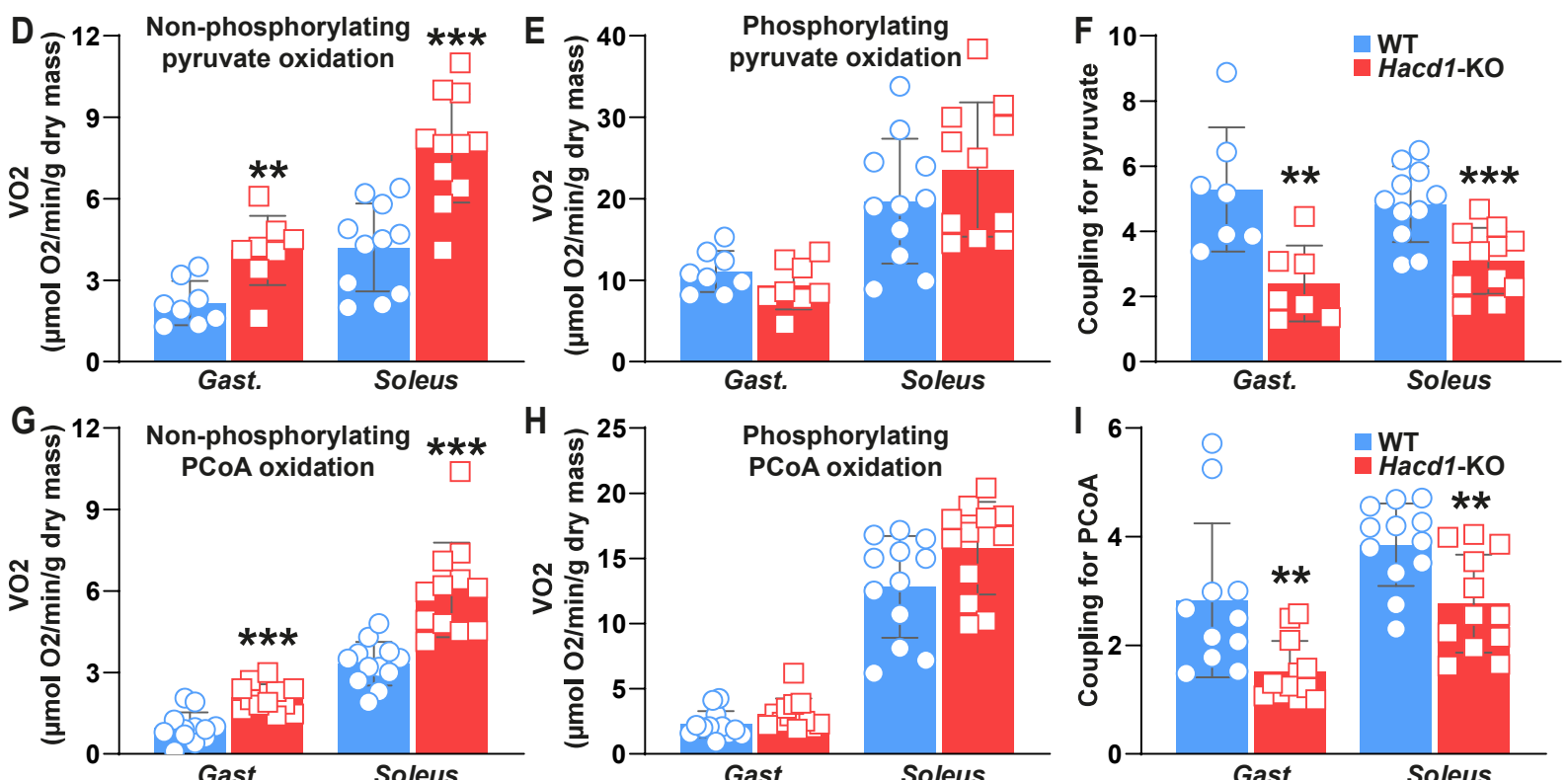
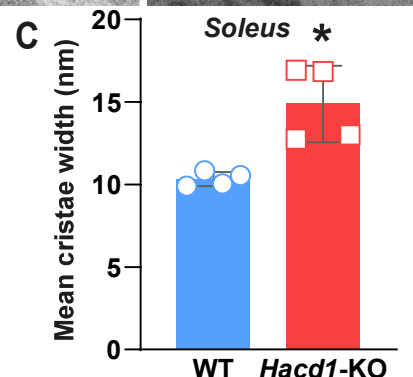
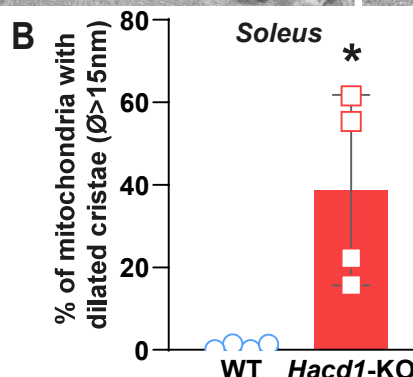
Supplemental Figure 1 | Metabolic parameters associated with protection against high-fat diet-induced obesity in *Hacd1*-KO mice. Related to Figure 1.

(A) Mean speed of spontaneous nocturnal locomotor activity. **(B)** Hematoxylin & Eosin-stained transverse sections of gonadal fat pads after 9 wk of high-fat diet (HFD), highlighting the contour of adipocytes. **(C)** Oil-Red-O-stained transverse sections of liver after 9 wk of HFD. **(D)** Mean daily food intake during the 9-wk period of HFD per mouse. **(E)** Cumulated energy intake during the 9-wk period of HFD. **(F)** Fecal lipid excretion after 8 wk of HFD. **(G)** Circadian energy expenditure measured by indirect calorimetry under normal diet (ND); the active period of night is shaded. Mean hourly energy expenditure during the assessment period is represented as histogram. **(H)** Feed efficiency during the 9-wk assessment period of ND. **(I-K)** *Ucp1* (**I**), *Ucp2* (**J**) and *Ucp3* (**K**) mRNA expression normalized by geometrical mean of three independent reference genes in superficial *gastrocnemius* muscle (*Gast.*), heart, liver, gonadal white adipose tissue (WAT) and brown adipose tissue (BAT) of *Hacd1*-KO mice, compared to WT mice set to 1.0. Scale bars represent 50 μ m in **B** and **C**. Error bars, \pm s.e.; * P < 0.05 and ** P < 0.01 versus respective WT values.



Supplemental Figure 2 | Metabolic changes of *Hacd1*-KO mice are restricted to skeletal muscle. Related to Figure 2.

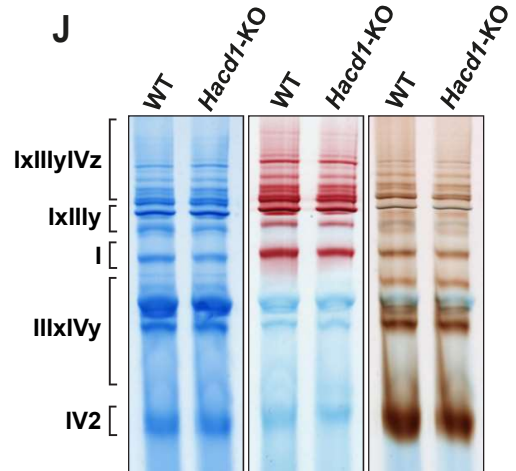
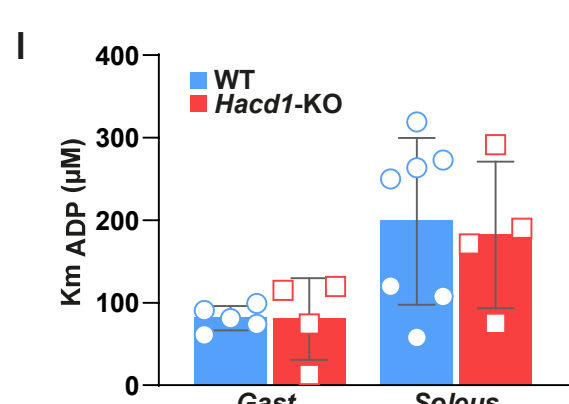
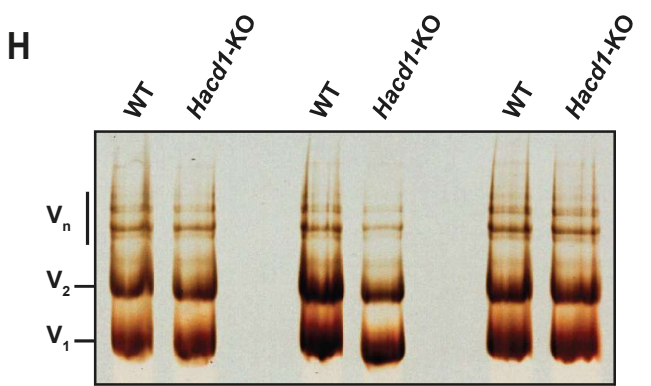
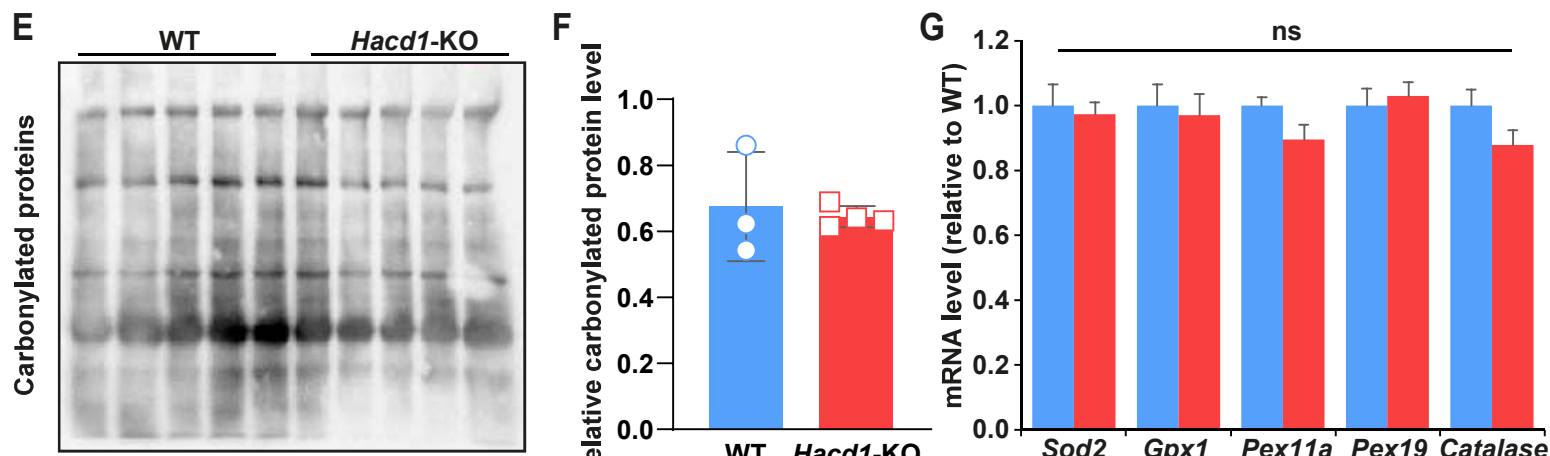
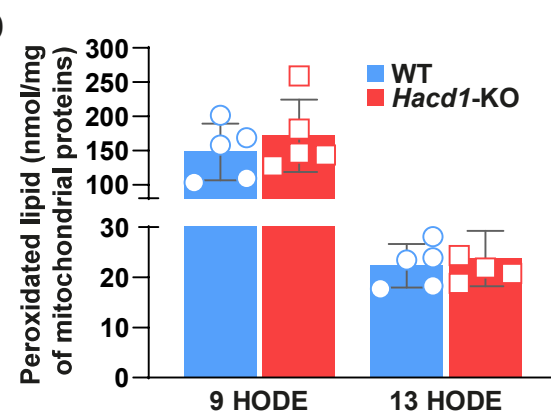
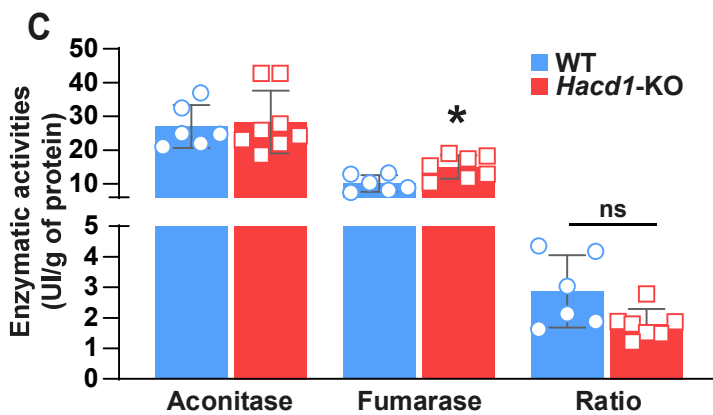
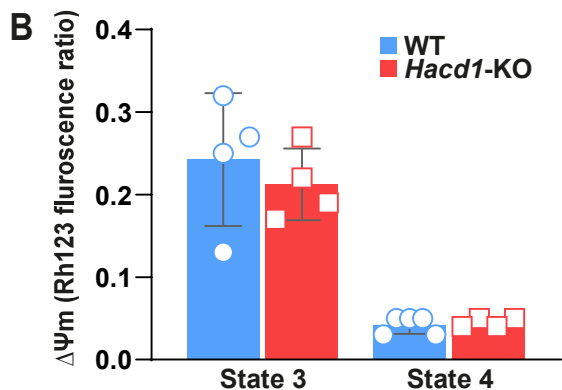
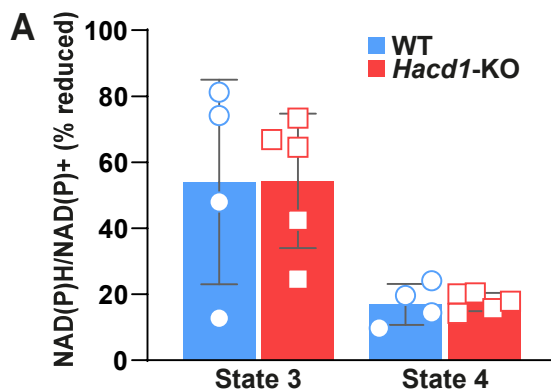
(A) *Ppargc1a*, *Ppargc1b*, *Tfam* and *Nrf1* mRNA expression normalized by the geometrical mean of three independent reference genes in superficial *gastrocnemius* muscle. **(B-C)** Representative immunoblots **(B)** and quantification **(C)** of CS and VDAC, normalized to the expression of β -Actin in heart, liver, white adipose tissue (WAT) and brown adipose tissue (BAT). **(D)** mRNA expression in superficial *gastrocnemius* muscle of a panel of genes involved in lipid metabolism, normalized by the geometrical mean of three independent reference genes. **(E)** mRNA expression of a panel of genes involved in mitochondrial biogenesis, lipid oxidation and lipogenesis, normalized by geometrical mean of three independent reference genes, in superficial *gastrocnemius* muscle (*Gast.*), heart, liver, gonadal white adipose tissue (WAT) and brown adipose tissue (BAT). **(F and G)** Gene ontology analysis and PANTHER protein set statistical enrichment analysis performed on the panel of the 96 proteins that are upregulated in the *tibialis anterior* muscle of *Hacd1*-KO mice, compared to WT mice. Error bars, \pm s.e.; * $P < 0.05$, ** $P < 0.01$ and *** $P < 0.001$ versus respective WT values.

A*Hacd1-KO*

Supplemental Figure 3 | Remodeled structure and modified respiratory parameters of skeletal muscle fibers of *Hacd1*-KO mice. Related to Figure 3.

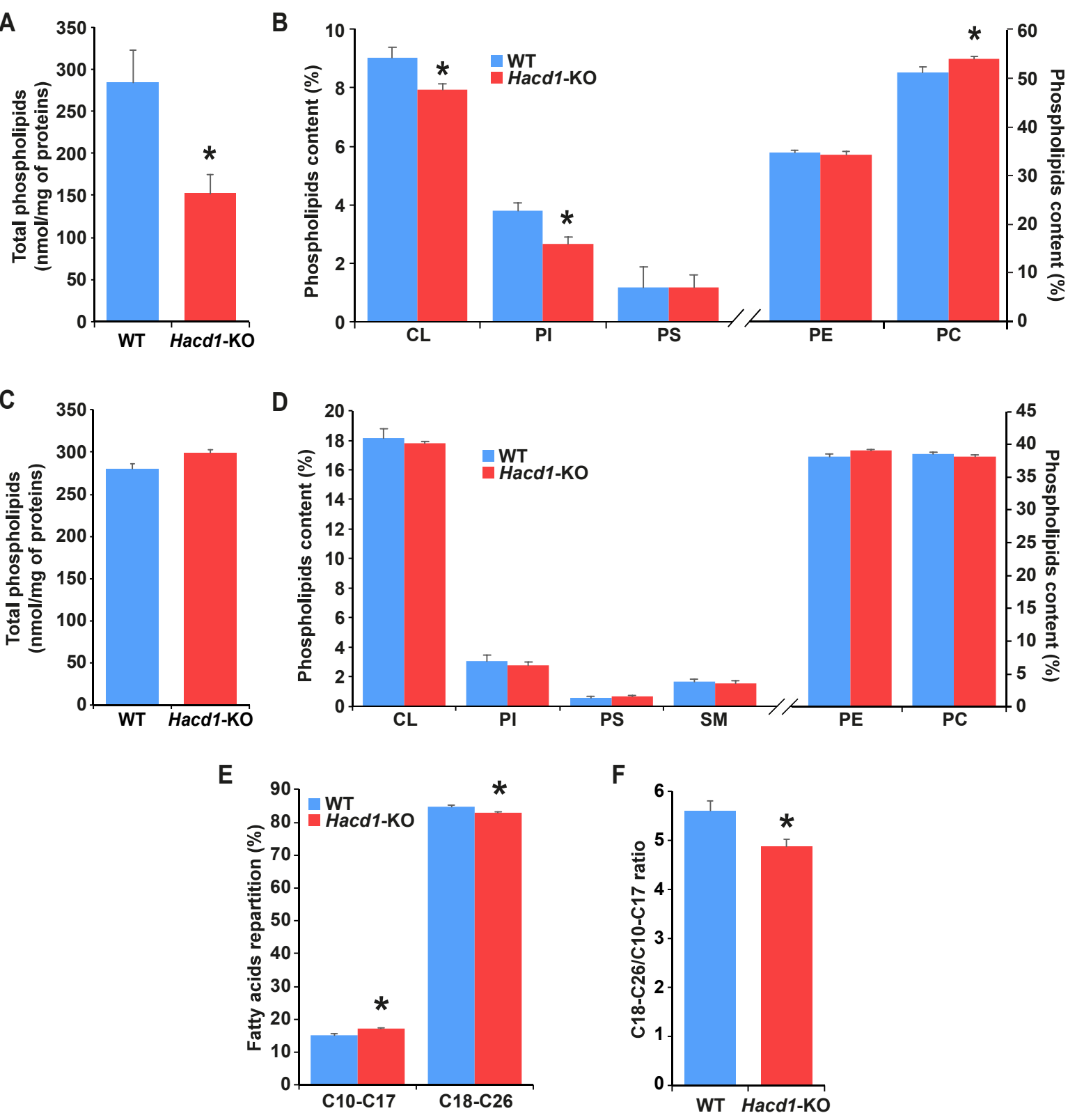
(A) Transmission electron microscopy of longitudinal sections of myofibers from *soleus* muscle. Images are from datasets taken at a low ($\times 2,500$; left panel), intermediate ($\times 10,000$; middle panel) and high ($\times 30,000$; right panel) magnification. The Z-line is delimited by arrows. Cristae are regular tubular-shaped invaginations (white arrow heads) of the inner mitochondrial membrane, unambiguously identified on the same plane than the outer mitochondrial membrane (black arrow heads). Excessive dilation of cristae tips (asterisk) is frequently observed in *Hacd1*-KO myofibers. **(B and C)** Morphometric quantification in *soleus* muscle of the percentage of mitochondria containing cristae with excessively dilated tips (maximal diameter >15 nm) **(B)** and the mean maximal diameter of the tubular segment of cristae **(C)**. **(D and E)** Non-phosphorylating **(D)** and phosphorylating **(E)** oxidation rate in the presence of pyruvate in permeabilized myofibers freshly isolated from superficial *gastrocnemius* (*Gast.*) and *soleus* muscles. **(F)** Mitochondrial coupling for pyruvate (Acceptor Control Ratio (ACR) of phosphorylating to non-phosphorylating oxidation rates of pyruvate from **D** and **E**). **(G and H)** Non-phosphorylating **(G)** and phosphorylating **(H)** oxidation rate in the presence of Palmitoyl-Coenzyme A (PCoA) in permeabilized myofibers freshly isolated from superficial *gastrocnemius* (*Gast.*) and *soleus* muscles. **(I)** Mitochondrial coupling for PCoA (ACR of phosphorylating to non-phosphorylating oxidation rates of PCoA from **G** and **H**). **(J and K)** Non-phosphorylating **(J)** and phosphorylating **(K)** respiration rates of saponin-permeabilized cardiac fibers in the presence of pyruvate. **(L)** Mitochondrial coupling of saponin-permeabilized cardiac fibers in the presence of pyruvate (ACR of phosphorylating to non-phosphorylating oxidation rates of pyruvate

from **J** and **K**). Scale bars in **A**: 100 nm. Error bars, \pm s.e.; * $P < 0.05$, ** $P < 0.01$ and *** $P < 0.001$ versus respective WT values.



Supplemental Figure 4 | Reduced mitochondrial coupling in muscle of *Hacd1*-KO mice is not associated with respiratory chain or ATP synthase dysfunction, nor oxidative stress. Related to Figure 3.

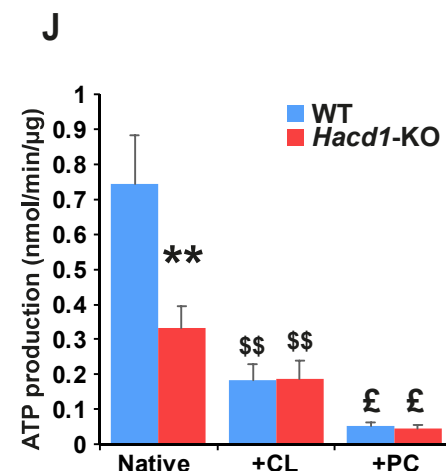
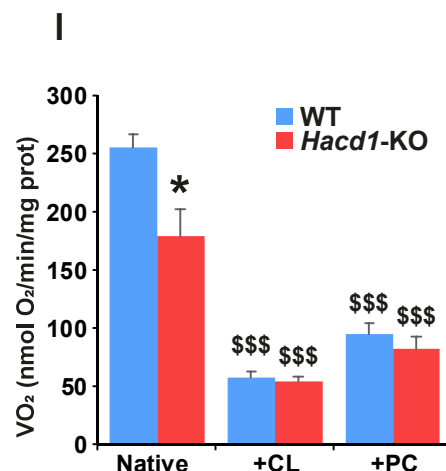
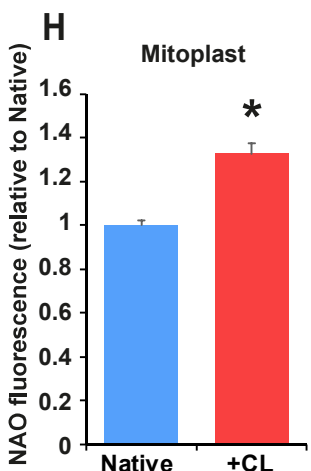
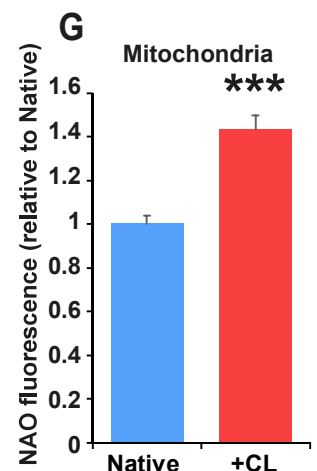
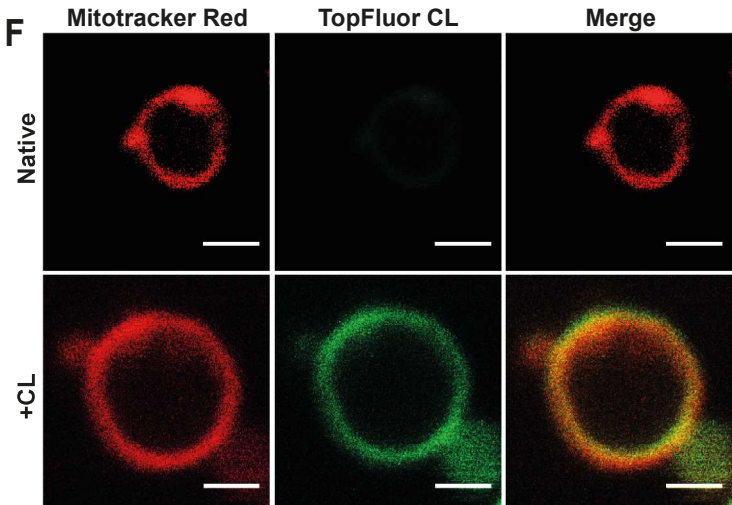
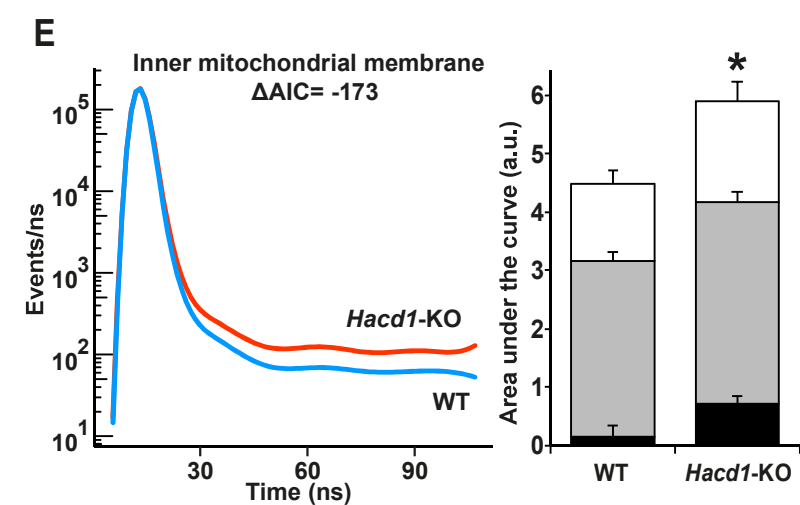
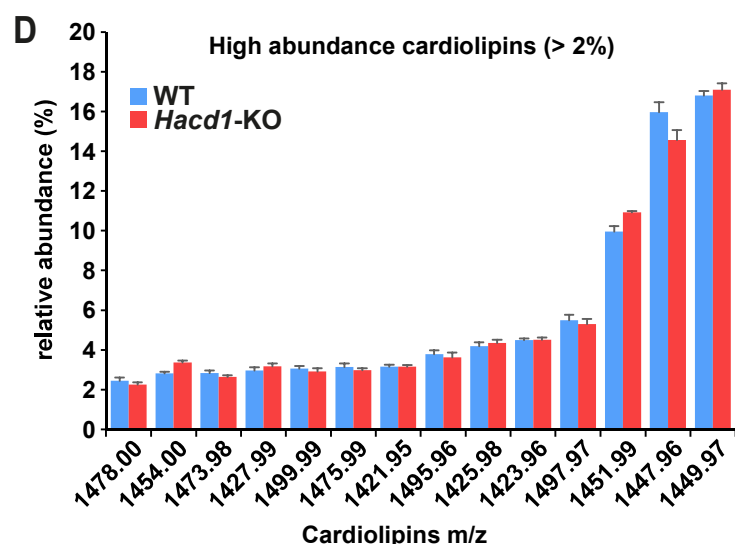
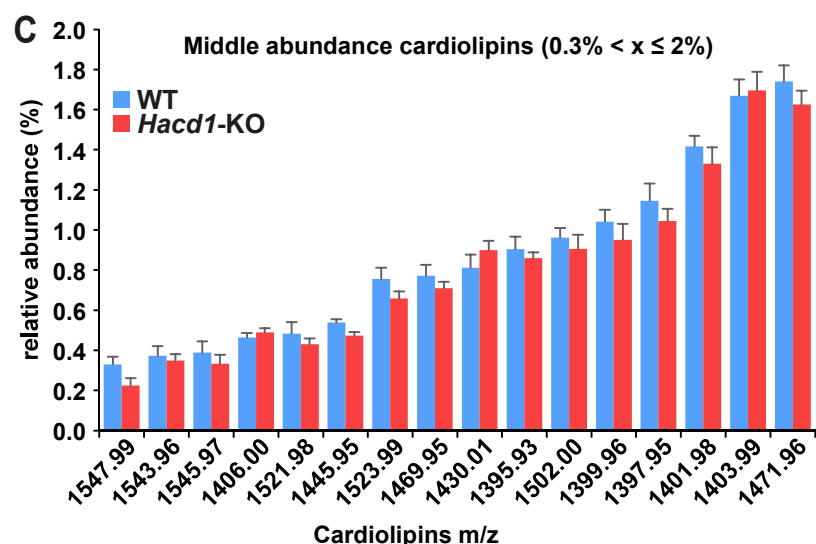
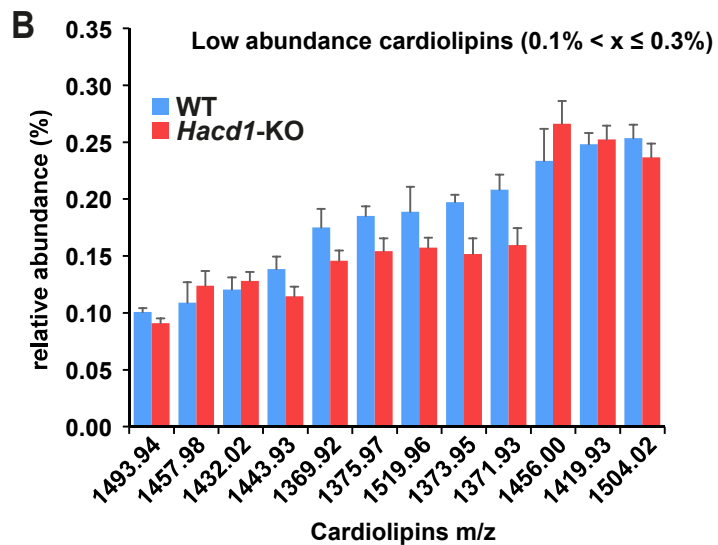
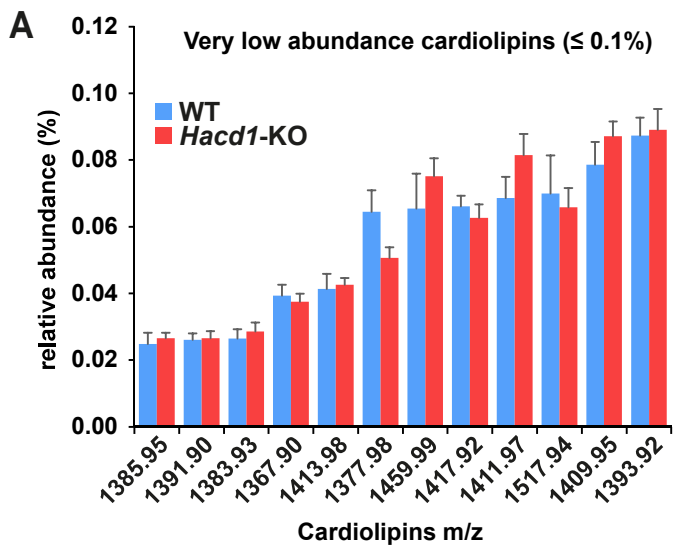
(A) NAD(P)H/NAD(P)⁺ ratio measured on isolated mitochondria from *tibialis anterior* muscle of WT and *Hacd1*-KO mice in state 4 (no ADP) and state 3 (2 mM ADP). **(B)** $\Delta\psi_m$ measured on isolated mitochondria from *tibialis anterior* muscle of WT and *Hacd1*-KO mice in state 4 (no ADP) and state 3 (2 mM ADP). **(C)** Aconitase and fumarase enzymatic activities and ratio of aconitase to fumarase activity in isolated mitochondria from *tibialis anterior* muscle. **(D)** 9-hydroxyoctadecadienoic acid (9-HODE) and 13-hydroxyoctadecadienoic acid (13-HODE) quantification in isolated mitochondria from *tibialis anterior* muscle. **(E and F)** Quantitative blotting of protein carbonylation in superficial *gastrocnemius* muscle. **(G)** *Sod2*, *Gpx1*, *Pex11a*, *Pex19* and *Catalase* mRNA expression normalized by geometrical mean of three independent reference genes in superficial *gastrocnemius* muscle. **(H)** In-gel activity of mitochondrial ATP synthase complexes isolated from the *tibialis anterior* muscle. **(I)** Apparent K_m of oxygen consumption for ADP on permeabilized fibers from superficial *gastrocnemius* (*Gast.*) and *soleus* muscles. **(J)** Analysis of the supramolecular organization of mitochondrial respiratory chain complexes in WT and *Hacd1*-KO mice. Mitochondria from the *tibialis anterior* muscle were analyzed by BN-PAGE, followed by Coomassie Brilliant Blue staining or In-gel enzyme activities (IGA) for complexes I or IV. The positions of respiratory chain complexes and supercomplexes are indicated to the left. (Representative image from three independent experiments.) Error bars, \pm s.e.; * $P < 0.05$ versus respective WT values.



Supplemental Figure 5 | Phospholipid and fatty acid quantification in mitochondria from *Hacd1*-KO mice. Related to Figure 4.

(A) Total phospholipid content of mitochondria isolated from the *tibialis anterior* muscle, normalized to the mitochondrial protein content. **(B)** Relative phospholipid species content of mitochondria isolated from the *tibialis anterior* muscle, normalized to the total content of mitochondrial phospholipids. **(C)** Total phospholipid content of mitochondria isolated from the heart, normalized to the mitochondrial protein content. **(D)** Relative phospholipid species content of mitochondria isolated from the heart, normalized to the total content of mitochondrial phospholipids. **(E and F)** Fatty acids repartition **(E)** and ratio of C18-26 to C10-17 **(F)** from total lipids of mitochondria isolated from the *tibialis anterior* muscle. CL = cardiolipins, PC = phosphatidylcholine, PE = phosphatidylethanolamine, PI = phosphatidylinositol, PS = phosphatidylserine, SM = sphingomyeline.

error bars, \pm s.e.; * $P < 0.05$ and ** $P < 0.01$ versus respective WT values.



Supplemental Figure 6 | Cardiolipin enrichment in mitochondria from *Hacd1*-KO mice. Related to Figure 4.

(A-D) Relative cardiolipins composition of mitochondria isolated from tibialis anterior muscle of *Hacd1*-KO mice, compared to WT mice. Each cardiolipin species is expressed as a percentage of total cardiolipin content and separated as very low ($<0.1\%$, **A**), low ($0.1\% < x \leq 0.3\%$, **B**), middle ($0.3\% < x \leq 2\%$, **C**) and high ($>2\%$, **D**) abundance. **(E)** TMA-DPH lifetime decay (curves) and mixing proportions (histograms) in the inner mitochondrial membrane, measured on mitoplasts from the *tibialis anterior* muscle. **(F)** Representative images of mitoplasts made from native mitochondria or after fusion of mitochondria with TopFluor-Cardiolipin (CL) vesicles and stained with Mitotracker Red. Scale bar: $1\mu\text{m}$. **(G and H)** Quantification of cardiolipin enrichment with Nonyl-Acridine Orange (NAO) staining on native mitochondria and after fusion with CL vesicles (**G**) and on mitoplasts isolated from the corresponding mitochondria (**H**). **(I and J)** Oxidation rate (**I**) and ATP production (**J**) measured on native isolated mitochondria from *tibialis anterior* muscle or after fusion with cardiolipin (+CL) or phosphatidylcholine (+PC) vesicles. $n = 5$ per group for **A-D**; error bars: \pm s.e.m.; multiple pair wise tests using Holm-Bonferroni method revealed no significant differences. ΔAIC = difference in the Akaike's Information Criterion (full analysis in Tables S5); error bars, \pm s.e.; * $P < 0.05$ and ** $P < 0.01$ versus respective WT values; \$\$ = P \leq 0.01 \text{ vs Native, } \$\$\$ = P \leq 0.001 \text{ vs Native, } \mathbb{P} = P \leq 0.05 \text{ vs +CL.}